PoS(ICRC2023)278

Mass Composition from 3 EeV to 100 EeV using the Depth of the Maximum of Air-Shower Profiles Estimated with Deep Learning using Surface Detector Data of the Pierre Auger Observatory

Jonas Glombitza[a,b,*] **for the Pierre Auger Collaboration**[c]

[a]*Erlangen Centre for Astroparticle Physics, Friedrich-Alexander-Universität Erlangen-Nürnberg, Erlangen, Germany*

[b]*III. Physikalisches Institut A, RWTH Aachen University, Aachen, Germany*

[c]*Observatorio Pierre Auger, Av. San Martín Norte 304, 5613 Malargüe, Argentina*
Full author list: https://www.auger.org/archive/authors_icrc_2023.html

E-mail: spokespersons@auger.org

We present a new analysis for estimating the depth of the maximum of air-shower profiles, X_{max}, to investigate the evolution of the ultra-high-energy cosmic ray mass composition from 3 to 100 EeV. We use a recently developed deep-learning-based technique for the reconstruction of X_{max} from the data of the surface detector of the Pierre Auger Observatory. To avoid systematic uncertainties arising from hadronic interaction models in the simulation of surface detector data, we calibrate the new reconstruction technique with observations of the fluorescence detector. Using the novel analysis, we have a 10-fold increase of statistics at $E > 5$ EeV with respect to fluorescence detector data. We are able, for the first time, to study the evolution of the mean and standard deviation of the X_{max} distributions up to 100 EeV.

We find an excellent agreement with fluorescence observations and confirm the increase of the mean logarithmic mass $\langle \ln(A) \rangle$ and a decrease of the X_{max} fluctuations with energy. The X_{max} measurement at the highest — so far inaccessible — energies is consistent with a pure mass composition and a mean logarithmic mass of around ~ 3 (estimated using the Sibyll 2.3d and the EPOS-LHC hadronic interaction models). Furthermore, with the increase in statistics, we find indications for a structure beyond a constant elongation rate in the evolution of X_{max}.

ICRC2023
38th International Cosmic Ray Conference
The Astroparticle Physics Conference

*Speaker

1. Introduction

In recent decades, substantial advancements have been made in the study of ultra-high-energy cosmic rays (UHECRs) due to the establishment of the Pierre Auger Observatory [1] and the Telescope Array Project [2]. The mass composition of these highly energetic particles, exceeding energies of 1 EeV (10^{18} eV), provide insights into our understanding of cosmic rays, in particular their acceleration, origin, and propagation [3].

The most precise measurement of the UHECR composition relies on measurements of the depth of the maximum of air-shower profiles ($X_{\max}$). By studying the mean $\langle X_{\max} \rangle$ and standard deviation $\sigma(X_{\max})$ of the $X_{\max}$ distributions as a function of energy, conclusions can be drawn on the evolution of the mean logarithmic mass $\langle \ln(A) \rangle$ and the composition mixing [4–7]. With increasing cosmic ray mass, the induced extensive air showers reach maximum higher in the atmosphere as the primary energy is divided between A sub-showers developing in parallel, translating to a smaller $X_{\max}$ in comparison to light particles. Additionally, fluctuations in the shower development average out, resulting in a smaller standard deviation $\sigma(X_{\max})$ of the $X_{\max}$ distributions.

Measurements of $X_{\max}$ can be performed by observations of the longitudinal shower development using fluorescence telescopes. These fluorescence observations enable accurate $X_{\max}$ reconstructions but are limited to dark nights and good weather conditions. In contrast, surface detector arrays feature duty cycles close to 100%, enabling measurements of UHECRs with high statistics. However, using this technique, $X_{\max}$ cannot be observed directly but is encoded in the temporal structure of the particle footprint, making the reconstruction challenging. Using observables designed by physicists, like the signal risetime, conclusions on the average change in composition can be obtained with good precision [8, 9].

The recent progress in deep learning and associated techniques based on deep neural networks open up vast and new possibilities for improved reconstructions in particle, astroparticle, and physics in general [10]. In this work, we present the application of a recently developed deep-learning-based reconstruction algorithm tailored to the situation of the world's largest cosmic ray observatory, the Pierre Auger Observatory. The algorithm exploits the time-dependent particle density recorded by the surface detector (SD) array of the observatory and is designed to reconstruct $X_{\max}$ on an event-by-event basis. After cross-calibrating the algorithm to observations of the Fluorescence Detector (FD), we show, for the first time, its application to the full SD data set. This leads to an increase in $X_{\max}$ statistics by a factor of 10 in comparison to FD analyses and enables us to measure $\langle X_{\max} \rangle$ and $\sigma(X_{\max})$ up to 10^{20} eV for the first time. We find excellent agreement with previous analyses and obtain new insights into the mass composition of UHECRs, in particular by finding indications for a characteristic structure in the evolution of the mean logarithmic mass above 10^{18} eV that correlates with the features in the energy spectrum.

2. Data

The Pierre Auger Observatory features a hybrid design combining an SD array covering 3,000 km^2 and the FD consisting of 27 telescopes overlooking the SD array from four sites. The SD comprises 1,600 water-Cherenkov detectors arranged in a triangular grid detecting the time-dependent particle density. Each SD station is equipped with three photomultiplier tubes (PMTs)
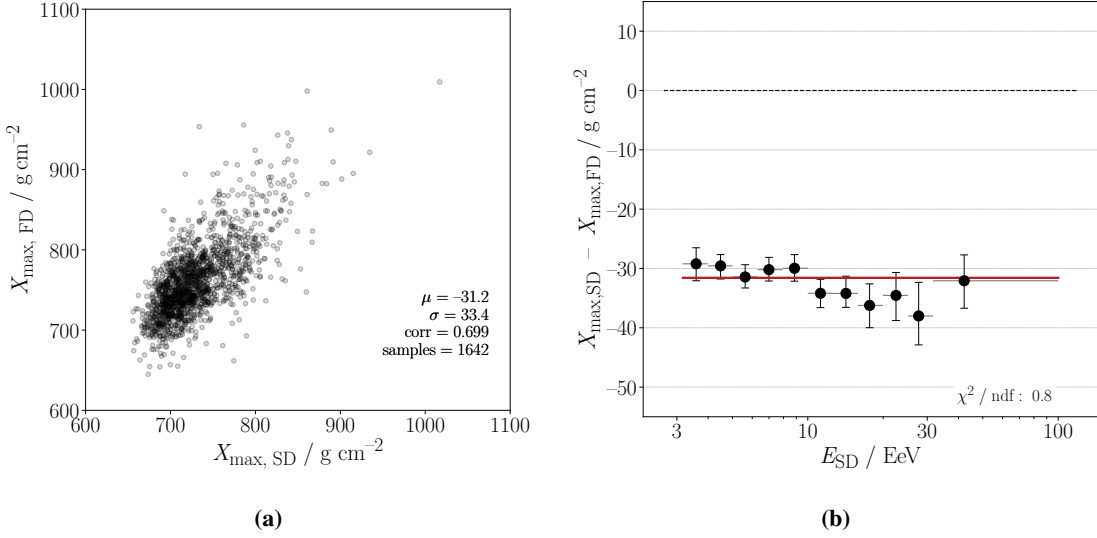
(a)   **(b)**

Figure 1: Calibration of the DNN using hybrid measurements. (a) Correlation between X_{max} reconstructed using the FD and the deep neural network. (b) Bias of the X_{max} reconstructed using the DNN with respect to the reconstruction of the fluorescence detector as a function of energy.

that detect the Cherenkov light induced by secondary particles traversing the water tanks. For each station, the measurement comprises an accurate determination of the arrival time of the first particles and a time-dependent signal measurement covering 3 μs in bins of 25 ns.

To ensure a high-quality selection, we use the standard SD selection [11], i.e., reject events below $10^{18.5}$ eV and zenith angles above 60°, and accept only events where each station in the hexagon surrounding the station with the largest signal is working. We further apply a fiducial selection derived using simulations to select only events that fall in a zenith range where the composition bias of the DNN between iron and proton is smaller than 10 g cm^{-2}. The cut is energy-dependent and removes events with geometries challenging to reconstruct using the SD. After selection, our data set consists of 48,824 events recorded with the SD array of the Pierre Auger Observatory, from January 1, 2004, to August 31, 2018.

For cross-calibration of the algorithm, a data set of *hybrid measurements* is also utilized to remove the dependency on the hadronic interaction models and detector effects. After performing the SD selection as described above, the FD selection [5] is applied, guaranteeing stable calibrations, good observation conditions, an adequate reconstruction of the Gaisser-Hillas profile, and an accurate reconstruction of X_{max} within the field of view of the telescope, ensuring that the event selection is unbiased, i.e., that the acceptance does not depend on X_{max}. The hybrid data set after cuts comprises 1,642 events measured between January 1, 2004, and December 31, 2017.

3. X_{max} reconstruction using deep learning

To reconstruct the depth of the shower maximum X_{max}, the time-dependent particle footprint measured at each triggered SD station is exploited using deep neural networks. The arrival times, as well as the measured signal traces, are used as input for the algorithm. In detail, we utilize two

different deep learning techniques, convolutional neural networks (CNNs) and Long Short-Term Memory networks (LSTMs) [12]. Whereas the LSTM layers are used to analyze and characterize the signal traces into features, the following convolutional part exploits these station-wise characteristics and the arrival times. This is done by employing hexagonal convolutions [13] to analyze the spatial and time-dependent information, taking advantage of the triangular structure of the surface array.

The network is trained using a comprehensive air-shower library [14] simulated using COR-SIKA [15] and $\overline{\text{Off}}\underline{\text{line}}$ [16]. The hadronic interaction model EPOS-LHC [17] was used. As training data, we used a composition as equal fractions of proton, helium, oxygen, and iron. During the training of the neural network, data augmentation techniques were applied to mimic realistic variations in operating conditions, such as broken PMTs or broken stations, as well as different states of the electronics. This augmentation significantly reduces the gap between simulations and data by making the simulations more realistic. For a comprehensive summary of the pre-processing, the network design, as well as the training, refer to Ref. [18].

When applied to simulations using the hadronic interaction models QGSJetII-04 and Sibyll2.3c, not used during training, in our studies [18], a bias of $\langle X_{\max} \rangle$ was found amounting up to -15 g cm^{-2}. In contrast, the estimations of $\sigma(X_{\max})$ as well as the methods' resolution, do not show a strong dependency on the interaction models. To remove the dependency on the interaction model used during the training, we calibrate the $X_{\max}$ reconstruction of the DNN to the $X_{\max}$ measurements of the FD.

The application to hybrid data is shown in Fig. 1. A strong correlation between the reconstructions can be seen in Fig. 1a, which amounts to a Pearson correlation of $\rho = 0.7$. This result is in excellent agreement with the correlation expected from simulation studies assuming the same energy spectrum and a composition scenario inferred using the FD data [6]. However, an offset of ≈ -31 g cm^{-2} between the SD and FD reconstruction is visible. This offset is larger than the one expected from simulation studies that predicted biases up to -15 g cm^{-2}. This large bias found in data reflects discrepancies between the current generation of hadronic interaction models and data, such as the modeling of the muonic component [19] as well as small remaining differences of the simulated detector response, including atmospheric models. Our simulation studies predicted any bias to be independent of energy, to a good approximation. As shown in Fig. 1b, no significant deviations from this expectation are visible in the data. Thus, we perform an energy-independent calibration of the SD $X_{\max}$. Nevertheless, we note that an energy-dependent linear fit also gives a good description of the observed bias. This finding propagates as an energy-dependent uncertainty into the systematic uncertainties of the $\langle X_{\max} \rangle$ measurement.

Since the resolution of the neural network, as well as $\sigma(X_{\max})$, does not show a strong dependence on the hadronic interaction model, we do not perform a calibration of the second moment. This finding is rooted in the fact that the fluctuations in $X_{\max}$ generally vary little between the models. Nevertheless, the small systematic differences found in the reconstruction of $\sigma(X_{\max})$ when applying the network to various compositions and interaction models are propagated into the systematic uncertainties of the $\sigma(X_{\max})$ measurement.
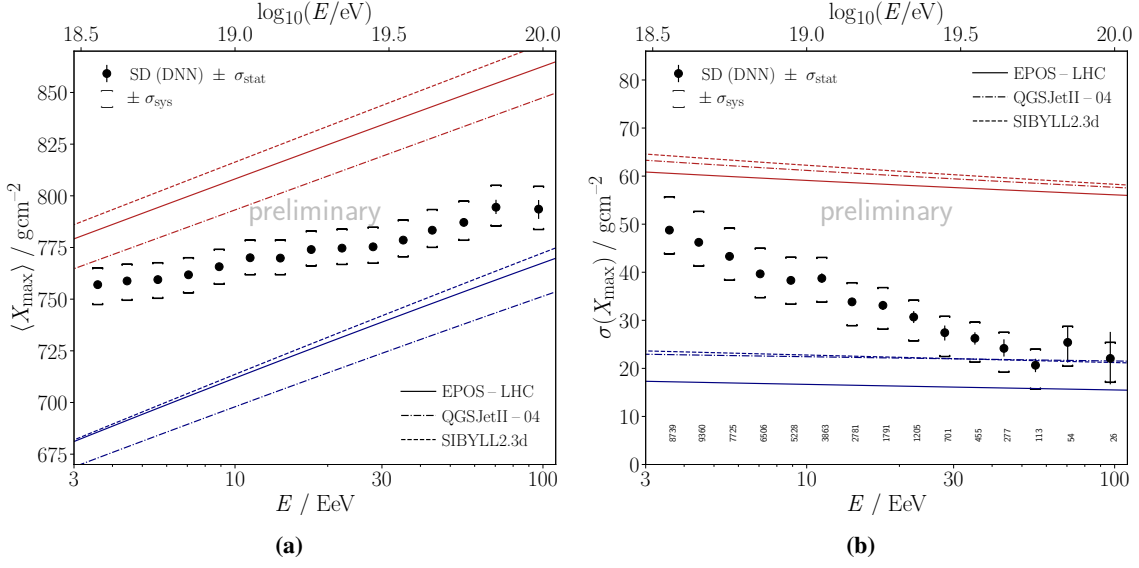
Figure 2: UHECR mass composition. (a) Average shower maximum and (b) the fluctuations of the shower maximum as determined using the DNN (black circles) as a function of energy. Red (blue) lines indicate hadronic model expectations for a pure proton (iron) composition.

4. Inferences on the UHECR mass composition using the Surface Detector

The inferences on the UHECR mass composition are based on the first and second moment of the X_{max} distributions (see Fig. 2) obtained using the deep-learning-based reconstruction of the SD data after cross-calibration with the FD data. With almost 50,000 events, this is the most comprehensive study of the mass composition between $10^{18.5}$ eV to 10^{20} eV based on X_{max}. The red (blue) lines in Fig. 2 indicate predictions from the hadronic interaction models EPOS-LHC, Sibyll2.3c [20], and QGSJetII-04 [21] for a pure proton (iron) composition. Errors bars indicate statistical uncertainties. The systematic uncertainties are visualized as brackets.

We show in Fig. 2a the measurement of $\langle X_{max} \rangle$ as a function of energy. The largest part of the systematic uncertainties is due to the uncertainty on the X_{max} scale [5] and the hybrid calibration of the deep neural network. Also, the ageing of the SD stations and diurnal variation contribute to the uncertainty, but these effects are comparatively small. A clear trend from a lighter to a heavier composition as a function of energy can be seen. The elongation rate amounts to $D_{10} = 24.1 \pm 1.2$ (stat.) ± 2.5 (sys.)g cm^{-2}/decade (compare Fig. 3a), where the systematic uncertainty is obtained by varying the performed hybrid calibration. This finding is in excellent agreement with previous studies based on FD data.

In Fig. 2b, we present the energy evolution of the fluctuations $\sigma(X_{max})$. Using the large statistics accumulated by the SD, we can, for the first time, extend this measurement up to 100 EeV. For the measurement of $\sigma(X_{max})$, the composition and interaction model bias found in simulations dominates the systematic uncertainties that are indicated by brackets. At the highest energies, in addition, effects of saturated stations, as well as detector ageing, contribute. At low energies, fluctuations of up to 50 g cm^{-2} are observed, indicating a relatively light and mixed composition. With increasing energy, the fluctuations decrease. Above 50 EeV, $\sigma(X_{max})$ is about 25 g cm^{-2},
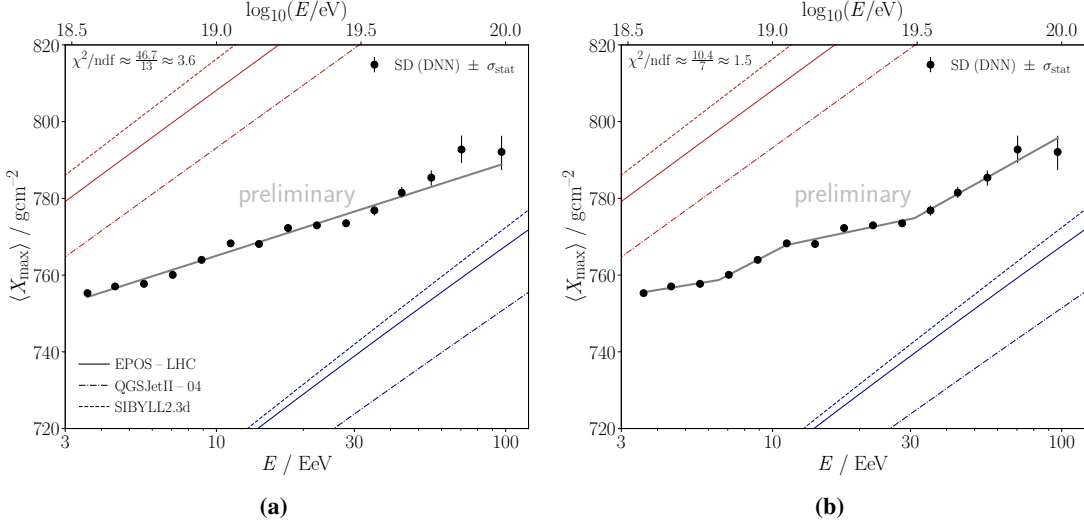
Figure 3: (a) Fit of a constant elongation rate to the SD data. (b) Model, featuring three breaks in the elongation rate, describing the identified structure in the SD data best.

indicating both a heavy and nearly pure composition. This strongly excludes a large fraction of protons and light nuclei at the highest energy and significantly excludes the cutoff observed in the energy spectrum to be formed by GZK protons. This observation is in very good agreement with the indications obtained using fluorescence observations [6, 22, 23].

4.1 Evidence for a characteristic structure in the energy evolution of the mass composition

The X_{max} reconstruction using the SD data allows us to perform high-statistics studies of the energy evolution of the first and second moment of the X_{max} distributions. This enlargement in statistics by a factor of 10 in comparison to previous analyses based on the FD significantly increases the potential to investigate changes in the $\langle X_{max} \rangle$ elongation rate. Though the elongation rate measured by the FD and the SD agrees well, the goodness of the straight-line fit of the SD is poor, $\chi^2/\text{ndf} = \frac{46.7}{13} \approx 3.6$. Therefore, the SD $\langle X_{max} \rangle$ evolution cannot be described with a constant elongation rate. A characteristic structure can be identified when fitting more complex models, suggesting three breaks in the elongation rate presented in Fig. 3b.

Within this model, the elongation rate changes from 12 ± 5 g cm^{-2}/decade to 39 ± 9 g cm^{-2}/decade at $E_0 = 6.5 \pm 0.6$ EeV. At an energy of $E_1 = 11 \pm 1.6$ EeV the elongation rate changes to 16 ± 3 g cm^{-2}/decade before reaching 42 ± 9 g cm^{-2}/decade above $E_2 = 31 \pm 5$ EeV. Using this model — featuring three breaks — the hypothesis of a constant elongation rate can be rejected by 4.6σ significance on a statistical basis. When including systematic uncertainties, by varying the data by the upper and lower bounds of the energy-dependent X_{max} systematics from the FD and the hybrid calibration, the significance reduces slightly to 4.4σ. In these tests, we varied the calibration functions (Fig. 1b), including the utilization of piece-wise linear calibration functions with the breaks fixed to the break positions found in the elongation rate.

A different null hypothesis, a model with two breaks at the lower energies, can be rejected at a significance of 2.6σ, including systematics. The statistics obtained with AugerPrime and its
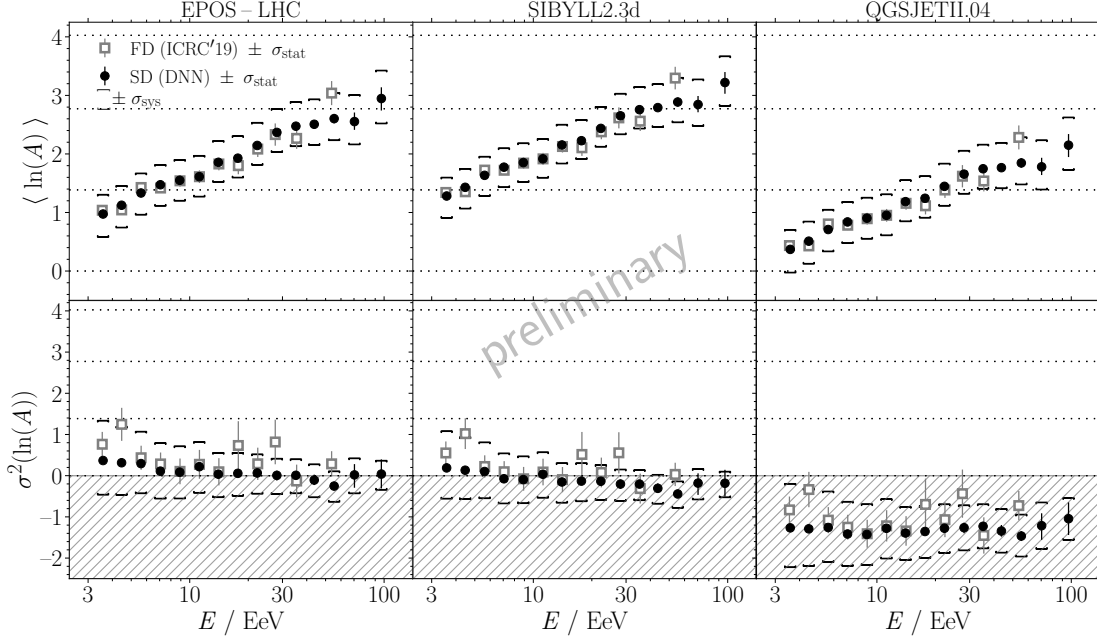
Figure 4: Energy evolution of the first two moments of the $\ln(A)$ distributions obtained from the conversion of the X_{max} moments [7] for the interaction models EPOS-LHC, Sibyl2.3c, and QGSJetII-04. We further compare our measurements to FD data from the same data-taking period [22], shown as open squares.

increased sensitivity, however, will provide new insights, also via a more precise hybrid calibration at high energies.

Our finding strongly indicates a change of the elongation rate beyond $10^{18.5}$ eV. Interestingly, the positions of the breaks found correlate with the positions of the ankle, instep, and suppression identified in the UHECR energy spectrum [24, 25].

4.2 Interpretation using hadronic interaction models

For interpreting the measurement, the first and second X_{max} moments can be converted to the moments of $\ln(A)$ using hadronic interaction models [7]. We show the evolution with the energy of the first two moments of $\ln(A)$ for the interaction models EPOS-LHC, Sibyl2.3c, and QGSJetII-04 in Fig. 4 for the SD data (black solid markers) and FD measurements (grey open markers) from the same data-taking period [22]. We find a remarkable agreement between both measurements. As expected, a very similar trend towards a heavier composition can be observed; also, the breaks identified in the evolution of $\langle X_{max} \rangle$ are naturally reflected in the $\langle \ln(A) \rangle$ inferences.

When examining the fluctuations in $\ln(A)$ (lower plot in Fig. 4), a pure composition can be identified over the whole energy range. Whereas inferences with EPOS-LHC and Sibyl2.3c are still in the physically allowed ranges of $\sigma(\ln(A))$, the negative fluctuation estimates with QGSJetII-04 disfavor the hadronic interaction model.

7

5. Summary

In this work, we have reported the application of a novel, deep-learning-based X_{max} reconstruction algorithm to almost 15 years of Auger SD data. With this new innovative technique, we have studied the mass composition of UHECR from $10^{18.5}$ eV up to 10^{20} eV. Due to the large exposure of the SD, the statistics in X_{max} compared to previous analyses are increased by a factor of 10. Using this large data set, the trend from a light to a heavier and purer composition with rising energy is confirmed. At the highest energies, we find small fluctuations in $\sigma(X_{max})$, excluding a considerable fraction of light nuclei in the UHECR composition. We additionally find evidence (4.4σ) for a characteristic structure beyond a constant elongation rate. The model describing our data best comprises three changes in the elongation rate that coincide with features of the energy spectrum.

With the future gain of statistics and the increased composition sensitivity of AugerPrime, paired with the advancements in innovative algorithms, we are awaiting further in-depth insights into the understanding of UHECRs and their mass composition.

References

[1] A. Aab *et al.* [Pierre Auger Coll.], Nucl. Instrum. Meth. A **798** (2015) 172.

[2] H. Kawai *et al.* [Telescope Array Coll.], Nucl. Phys. B **175-176** (2008) 221.

[3] K. H. Kampert, M. Unger, Astropart. Phys., **35** (2002) 660.

[4] A. Abraham *et al.* [Pierre Auger Coll.], Phys. Rev. Lett., **104** (2010) 091101.

[5] A. Aab *et al.* [Pierre Auger Coll.], Phys. Rev. D **90** (2014) 122005.

[6] A. Aab *et al.* [Pierre Auger Coll.], Phys. Rev. D **90** (2014) 122006.

[7] A. Aab *et al.* [Pierre Auger Coll.], JCAP **02** (2013) 026.

[8] A. Aab *et al.* [Pierre Auger Coll.], Phys. Rev. D **96** (2017) 122003.

[9] C. J. T. Peixoto for the Pierre Auger Collaboration, PoS, **358** (2019) 440.

[10] M. Erdmann, J. Glombitza, G. Kasieczka, U. Klemradt, World Scientific, 2021.

[11] A. Aab *et al.* [Pierre Auger Coll.], JINST **15** (2020) P10021.

[12] S. Hochreiter, J. Schmidhuber, Neural Computation **9(8)** (1997) 1735–1780.

[13] E. Hoogeboom, J.W.T. Peters, T.S. Cohen, M. Welling, [ArXiv:1803.02108].

[14] E. Santos for the Pierre Auger Coll., these proceedings.

[15] D. Heck *et al.*, Forschungszentrum Karlsruhe Report FZKA (1998) 6019.

[16] S. Argiro *et al.*, Nucl. Instrum. Meth. A **580** (2007) 1485.

[17] T. Pierog *et al.*, Phys. Rev. D **92** (2015) 034906.

[18] A. Aab *et al.* [Pierre Auger Coll.], JINST **16** (2021) P07019.

[19] A. Aab *et al.* [Pierre Auger Coll.], Phys. Rev. D **90** (2014) 012012.

[20] F. Riehn *et al.*, PoS, **301** (2018).

[21] S. Ostapchenko, Phys. Rev. D **72** (2006) 14.

[22] A. Yushkov on behalf of the Pierre Auger Coll., PoS **ICRC** (2019) 482.

[23] A. Aab *et al.* [Pierre Auger Coll.] JCAP **04** (2017) 038

[24] A. Aab *et al.*, Phys. Rev. Lett. **125** (2020) 121106.

[25] A. Aab *et al.*, Phys. Rev. D **102** (2020) 062005.

[26] A. Castellina for the Pierre Auger Coll. EPJ Web of Conferences, **210** (2019) 06002

[27] P. Abreu *et al.* [Pierre Auger Coll.], [ArXiv:1107.4806].

[28] A. Aab *et al.* [Pierre Auger Coll.], Phys. Rev. D **91** (2015) 032003.

The Pierre Auger Collaboration
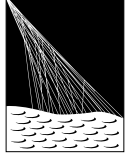
A. Abdul Halim[13], P. Abreu[72], M. Aglietta[54,52], I. Allekotte[1], K. Almeida Cheminant[70], A. Almela[7,12], R. Aloisio[45,46], J. Alvarez-Muñiz[79], J. Ammerman Yebra[79], G.A. Anastasi[54,52], L. Anchordoqui[86], B. Andrada[7], S. Andringa[72], C. Aramo[50], P.R. Araújo Ferreira[42], E. Arnone[63,52], J. C. Arteaga Velázquez[67], H. Asorey[7], P. Assis[72], G. Avila[11], E. Avocone[57,46], A.M. Badescu[75], A. Bakalova[32], A. Balaceanu[73], F. Barbato[45,46], A. Bartz Mocellin[85], J.A. Bellido[13,69], C. Berat[36], M.E. Bertaina[63,52], G. Bhatta[70], M. Bianciotto[63,52], P.L. Biermann[h], V. Binet[5], K. Bismark[39,7], T. Bister[80,81], J. Biteau[37], J. Blazek[32], C. Bleve[36], J. Blümer[41], M. Boháčová[32], D. Boncioli[57,46], C. Bonifazi[8,26], L. Bonneau Arbeletche[21], N. Borodai[70], J. Brack[j], P.G. Brichetto Orchera[7], F.L. Briechle[42], A. Bueno[78], S. Buitink[15], M. Buscemi[47,61], M. Büsken[39,7], A. Bwembya[80,81], K.S. Caballero-Mora[66], S. Cabana-Freire[79], L. Caccianiga[59,49], I. Caracas[38], R. Caruso[58,47], A. Castellina[54,52], F. Catalani[18], G. Cataldi[48], L. Cazon[79], M. Cerda[10], A. Cermenati[45,46], J.A. Chinellato[21], J. Chudoba[32], L. Chytka[33], R.W. Clay[13], A.C. Cobos Cerutti[6], R. Colalillo[60,50], A. Coleman[90], M.R. Coluccia[48], R. Conceição[72], A. Condorelli[37], G. Consolati[49,55], M. Conte[56,48], F. Convenga[41], D. Correia dos Santos[28], P.J. Costa[72], C.E. Covault[84], M. Cristinziani[44], C.S. Cruz Sanchez[3], S. Dasso[4,2], K. Daumiller[41], B.R. Dawson[13], R.M. de Almeida[28], J. de Jesús[7,41], S.J. de Jong[80,81], J.R.T. de Mello Neto[26,27], I. De Mitri[45,46], J. de Oliveira[17], D. de Oliveira Franco[21], F. de Palma[56,48], V. de Souza[19], E. De Vito[56,48], A. Del Popolo[58,47], O. Deligny[34], N. Denner[32], L. Deval[41,7], A. di Matteo[52], M. Dobre[73], C. Dobrigkeit[21], J.C. D'Olivo[68], L.M. Domingues Mendes[72], J.C. dos Anjos, R.C. dos Anjos[25], J. Ebr[32], F. Ellwanger[41], M. Emam[80,81], R. Engel[39,41], I. Epicoco[56,48], M. Erdmann[42], A. Etchegoyen[7,12], C. Evoli[45,46], H. Falcke[80,82,81], J. Farmer[89], G. Farrar[88], A.C. Fauth[21], N. Fazzini[e], F. Feldbusch[40], F. Fenu[41,d], A. Fernandes[72], B. Fick[87], J.M. Figueira[7], A. Filipčič[77,76], T. Fitoussi[41], B. Flaggs[90], T. Fodran[80], T. Fujii[89,f], A. Fuster[7,12], C. Galea[80], C. Galelli[59,49], B. García[6], C. Gaudu[38], H. Gemmeke[40], F. Gesualdi[7,41], A. Gherghel-Lascu[73], P.L. Ghia[34], U. Giaccari[48], M. Giammarchi[49], J. Glombitza[42,g], F. Gobbi[10], F. Gollan[7], G. Golup[1], M. Gómez Berisso[1], P.F. Gómez Vitale[11], J.P. Gongora[11], J.M. González[1], N. González[7], I. Goos[1], D. Góra[70], A. Gorgi[54,52], M. Gottowik[79], T.D. Grubb[13], F. Guarino[60,50], G.P. Guedes[22], E. Guido[44], S. Hahn[39], P. Hamal[32], M.R. Hampel[7], P. Hansen[3], D. Harari[1], V.M. Harvey[13], A. Haungs[41], T. Hebbeker[42], C. Hojvat[e], J.R. Hörandel[80,81], P. Horvath[33], M. Hrabovský[33], T. Huege[41,15], A. Insolia[58,47], P.G. Isar[74], P. Janecek[32], J.A. Johnsen[85], J. Jurysek[32], A. Kääpä[38], K.H. Kampert[38], B. Keilhauer[41], A. Khakurdikar[80], V.V. Kizakke Covilakam[7,41], H.O. Klages[41], M. Kleifges[40], F. Knapp[39], N. Kunka[40], B.L. Lago[16], N. Langner[42], M.A. Leigui de Oliveira[24], Y Lema-Capeans[79], V. Lenok[39], A. Letessier-Selvon[35], I. Lhenry-Yvon[34], D. Lo Presti[58,47], L. Lopes[72], L. Lu[91], Q. Luce[39], J.P. Lundquist[76], A. Machado Payeras[21], M. Majercakova[32], D. Mandat[32], B.C. Manning[13], P. Mantsch[e], S. Marafico[34], F.M. Mariani[59,49], A.G. Mariazzi[3], I.C. Mariş[14], G. Marsella[61,47], D. Martello[56,48], S. Martinelli[41,7], O. Martínez Bravo[64], M.A. Martins[79], M. Mastrodicasa[57,46], H.J. Mathes[41], J. Matthews[a], G. Matthiae[62,51], E. Mayotte[85,38], S. Mayotte[85], P.O. Mazur[e], G. Medina-Tanco[68], J. Meinert[38], D. Melo[7], A. Menshikov[40], C. Merx[41], S. Michal[33], M.I. Micheletti[5], L. Miramonti[59,49], S. Mollerach[1], F. Montanet[36], L. Morejon[38], C. Morello[54,52], A.L. Müller[32], K. Mulrey[80,81], R. Mussa[52], M. Muzio[88], W.M. Namasaka[38], S. Negi[32], L. Nellen[68], K. Nguyen[87], G. Nicora[9], M. Niculescu-Oglinzanu[73], M. Niechciol[44], D. Nitz[87], D. Nosek[31], V. Novotny[31], L. Nožka[33], A Nucita[56,48], L.A. Núñez[30], C. Oliveira[19], M. Palatka[32], J. Pallotta[9], S. Panja[32], G. Parente[79], T. Paulsen[38], J. Pawlowsky[38], M. Pech[32], J. Pękala[70], R. Pelayo[65], L.A.S. Pereira[23], E.E. Pereira Martins[39,7], J. Perez Armand[20], C. Pérez Bertolli[7,41], L. Perrone[56,48], S. Petrera[45,46], C. Petrucci[57,46], T. Pierog[41], M. Pimenta[72], M. Platino[7], B. Pont[80], M. Pothast[81,80], M. Pourmohammad Shahvar[61,47], P. Privitera[89], M. Prouza[32], A. Puyleart[87], S. Querchfeld[38], J. Rautenberg[38], D. Ravignani[7], M. Reininghaus[39], J. Ridky[32], F. Riehn[79], M. Risse[44], V. Rizi[57,46], W. Rodrigues de Carvalho[80], E. Rodriguez[7,41], J. Rodriguez Rojo[11], M.J. Roncoroni[7], S. Rossoni[43], M. Roth[41], E. Roulet[1], A.C. Rovero[4], P. Ruehl[44], A. Saftoiu[73], M. Saharan[80], F. Salamida[57,46], H. Salazar[64], G. Salina[51], J.D. Sanabria Gomez[30], F. Sánchez[7], E.M. Santos[20], E. Santos[32],

F. Sarazin[85], R. Sarmento[72], R. Sato[11], P. Savina[91], C.M. Schäfer[41], V. Scherini[56,48], H. Schieler[41], M. Schimassek[34], M. Schimp[38], F. Schlüter[41], D. Schmidt[39], O. Scholten[15,i], H. Schoorlemmer[80,81], P. Schovánek[32], F.G. Schröder[90,41], J. Schulte[42], T. Schulz[41], S.J. Sciutto[3], M. Scornavacche[7,41], A. Segreto[53,47], S. Sehgal[38], S.U. Shivashankara[76], G. Sigl[43], G. Silli[7], O. Sima[73,b], F. Simon[40], R. Smau[73], R. Šmída[89], P. Sommers[k], J.F. Soriano[86], R. Squartini[10], M. Stadelmaier[32], D. Stanca[73], S. Stanič[76], J. Stasielak[70], P. Stassi[36], S. Strähnz[39], M. Straub[42], M. Suárez-Durán[14], T. Suomijärvi[37], A.D. Supanitsky[7], Z. Svozilikova[32], Z. Szadkowski[71], A. Tapia[29], C. Taricco[63,52], C. Timmermans[81,80], O. Tkachenko[41], P. Tobiska[32], C.J. Todero Peixoto[18], B. Tomé[72], Z. Torrès[36], A. Travaini[10], P. Travnicek[32], C. Trimarelli[57,46], M. Tueros[3], M. Unger[41], L. Vaclavek[33], M. Vacula[33], J.F. Valdés Galicia[68], L. Valore[60,50], E. Varela[64], A. Vásquez-Ramírez[30], D. Veberič[41], C. Ventura[27], I.D. Vergara Quispe[3], V. Verzi[51], J. Vicha[32], J. Vink[83], J. Vlastimil[32], S. Vorobiov[76], C. Watanabe[26], A.A. Watson[c], A. Weindl[41], L. Wiencke[85], H. Wilczyński[70], D. Wittkowski[38], B. Wundheiler[7], B. Yue[38], A. Yushkov[32], O. Zapparrata[14], E. Zas[79], D. Zavrtanik[76,77], M. Zavrtanik[77,76]

——————— • ———————
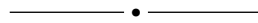
[1] Centro Atómico Bariloche and Instituto Balseiro (CNEA-UNCuyo-CONICET), San Carlos de Bariloche, Argentina

[2] Departamento de Física and Departamento de Ciencias de la Atmósfera y los Océanos, FCEyN, Universidad de Buenos Aires and CONICET, Buenos Aires, Argentina

[3] IFLP, Universidad Nacional de La Plata and CONICET, La Plata, Argentina

[4] Instituto de Astronomía y Física del Espacio (IAFE, CONICET-UBA), Buenos Aires, Argentina

[5] Instituto de Física de Rosario (IFIR) – CONICET/U.N.R. and Facultad de Ciencias Bioquímicas y Farmacéuticas U.N.R., Rosario, Argentina

[6] Instituto de Tecnologías en Detección y Astropartículas (CNEA, CONICET, UNSAM), and Universidad Tecnológica Nacional – Facultad Regional Mendoza (CONICET/CNEA), Mendoza, Argentina

[7] Instituto de Tecnologías en Detección y Astropartículas (CNEA, CONICET, UNSAM), Buenos Aires, Argentina

[8] International Center of Advanced Studies and Instituto de Ciencias Físicas, ECyT-UNSAM and CONICET, Campus Miguelete – San Martín, Buenos Aires, Argentina

[9] Laboratorio Atmósfera – Departamento de Investigaciones en Láseres y sus Aplicaciones – UNIDEF (CITEDEF-CONICET), Argentina

[10] Observatorio Pierre Auger, Malargüe, Argentina

[11] Observatorio Pierre Auger and Comisión Nacional de Energía Atómica, Malargüe, Argentina

[12] Universidad Tecnológica Nacional – Facultad Regional Buenos Aires, Buenos Aires, Argentina

[13] University of Adelaide, Adelaide, S.A., Australia

[14] Université Libre de Bruxelles (ULB), Brussels, Belgium

[15] Vrije Universiteit Brussels, Brussels, Belgium

[16] Centro Federal de Educação Tecnológica Celso Suckow da Fonseca, Petropolis, Brazil

[17] Instituto Federal de Educação, Ciência e Tecnologia do Rio de Janeiro (IFRJ), Brazil

[18] Universidade de São Paulo, Escola de Engenharia de Lorena, Lorena, SP, Brazil

[19] Universidade de São Paulo, Instituto de Física de São Carlos, São Carlos, SP, Brazil

[20] Universidade de São Paulo, Instituto de Física, São Paulo, SP, Brazil

[21] Universidade Estadual de Campinas, IFGW, Campinas, SP, Brazil

[22] Universidade Estadual de Feira de Santana, Feira de Santana, Brazil

[23] Universidade Federal de Campina Grande, Centro de Ciencias e Tecnologia, Campina Grande, Brazil

[24] Universidade Federal do ABC, Santo André, SP, Brazil

[25] Universidade Federal do Paraná, Setor Palotina, Palotina, Brazil

[26] Universidade Federal do Rio de Janeiro, Instituto de Física, Rio de Janeiro, RJ, Brazil

[27] Universidade Federal do Rio de Janeiro (UFRJ), Observatório do Valongo, Rio de Janeiro, RJ, Brazil

[28] Universidade Federal Fluminense, EEIMVR, Volta Redonda, RJ, Brazil

[29] Universidad de Medellín, Medellín, Colombia

[30] Universidad Industrial de Santander, Bucaramanga, Colombia

[31] Charles University, Faculty of Mathematics and Physics, Institute of Particle and Nuclear Physics, Prague, Czech Republic

[32] Institute of Physics of the Czech Academy of Sciences, Prague, Czech Republic

[33] Palacky University, Olomouc, Czech Republic

[34] CNRS/IN2P3, IJCLab, Université Paris-Saclay, Orsay, France

[35] Laboratoire de Physique Nucléaire et de Hautes Energies (LPNHE), Sorbonne Université, Université de Paris, CNRS-IN2P3, Paris, France

[36] Univ. Grenoble Alpes, CNRS, Grenoble Institute of Engineering Univ. Grenoble Alpes, LPSC-IN2P3, 38000 Grenoble, France

[37] Université Paris-Saclay, CNRS/IN2P3, IJCLab, Orsay, France

[38] Bergische Universität Wuppertal, Department of Physics, Wuppertal, Germany

[39] Karlsruhe Institute of Technology (KIT), Institute for Experimental Particle Physics, Karlsruhe, Germany

[40] Karlsruhe Institute of Technology (KIT), Institut für Prozessdatenverarbeitung und Elektronik, Karlsruhe, Germany

[41] Karlsruhe Institute of Technology (KIT), Institute for Astroparticle Physics, Karlsruhe, Germany

[42] RWTH Aachen University, III. Physikalisches Institut A, Aachen, Germany

[43] Universität Hamburg, II. Institut für Theoretische Physik, Hamburg, Germany

[44] Universität Siegen, Department Physik – Experimentelle Teilchenphysik, Siegen, Germany

[45] Gran Sasso Science Institute, L'Aquila, Italy

[46] INFN Laboratori Nazionali del Gran Sasso, Assergi (L'Aquila), Italy

[47] INFN, Sezione di Catania, Catania, Italy

[48] INFN, Sezione di Lecce, Lecce, Italy

[49] INFN, Sezione di Milano, Milano, Italy

[50] INFN, Sezione di Napoli, Napoli, Italy

[51] INFN, Sezione di Roma "Tor Vergata", Roma, Italy

[52] INFN, Sezione di Torino, Torino, Italy

[53] Istituto di Astrofisica Spaziale e Fisica Cosmica di Palermo (INAF), Palermo, Italy

[54] Osservatorio Astrofisico di Torino (INAF), Torino, Italy

[55] Politecnico di Milano, Dipartimento di Scienze e Tecnologie Aerospaziali , Milano, Italy

[56] Università del Salento, Dipartimento di Matematica e Fisica "E. De Giorgi", Lecce, Italy

[57] Università dell'Aquila, Dipartimento di Scienze Fisiche e Chimiche, L'Aquila, Italy

[58] Università di Catania, Dipartimento di Fisica e Astronomia "Ettore Majorana", Catania, Italy

[59] Università di Milano, Dipartimento di Fisica, Milano, Italy

[60] Università di Napoli "Federico II", Dipartimento di Fisica "Ettore Pancini", Napoli, Italy

[61] Università di Palermo, Dipartimento di Fisica e Chimica "E. Segrè", Palermo, Italy

[62] Università di Roma "Tor Vergata", Dipartimento di Fisica, Roma, Italy

[63] Università Torino, Dipartimento di Fisica, Torino, Italy

[64] Benemérita Universidad Autónoma de Puebla, Puebla, México

[65] Unidad Profesional Interdisciplinaria en Ingeniería y Tecnologías Avanzadas del Instituto Politécnico Nacional (UPIITA-IPN), México, D.F., México

[66] Universidad Autónoma de Chiapas, Tuxtla Gutiérrez, Chiapas, México

[67] Universidad Michoacana de San Nicolás de Hidalgo, Morelia, Michoacán, México

[68] Universidad Nacional Autónoma de México, México, D.F., México

[69] Universidad Nacional de San Agustin de Arequipa, Facultad de Ciencias Naturales y Formales, Arequipa, Peru

[70] Institute of Nuclear Physics PAN, Krakow, Poland

[71] University of Łódź, Faculty of High-Energy Astrophysics,Łódź, Poland

[72] Laboratório de Instrumentação e Física Experimental de Partículas – LIP and Instituto Superior Técnico – IST, Universidade de Lisboa – UL, Lisboa, Portugal

[73] "Horia Hulubei" National Institute for Physics and Nuclear Engineering, Bucharest-Magurele, Romania

[74] Institute of Space Science, Bucharest-Magurele, Romania

[75] University Politehnica of Bucharest, Bucharest, Romania

[76] Center for Astrophysics and Cosmology (CAC), University of Nova Gorica, Nova Gorica, Slovenia

[77] Experimental Particle Physics Department, J. Stefan Institute, Ljubljana, Slovenia

[78] Universidad de Granada and C.A.F.P.E., Granada, Spain

[79] Instituto Galego de Física de Altas Enerxías (IGFAE), Universidade de Santiago de Compostela, Santiago de Compostela, Spain

[80] IMAPP, Radboud University Nijmegen, Nijmegen, The Netherlands

[81] Nationaal Instituut voor Kernfysica en Hoge Energie Fysica (NIKHEF), Science Park, Amsterdam, The Netherlands

[82] Stichting Astronomisch Onderzoek in Nederland (ASTRON), Dwingeloo, The Netherlands

[83] Universiteit van Amsterdam, Faculty of Science, Amsterdam, The Netherlands

[84] Case Western Reserve University, Cleveland, OH, USA

[85] Colorado School of Mines, Golden, CO, USA

[86] Department of Physics and Astronomy, Lehman College, City University of New York, Bronx, NY, USA

[87] Michigan Technological University, Houghton, MI, USA

[88] New York University, New York, NY, USA

[89] University of Chicago, Enrico Fermi Institute, Chicago, IL, USA

[90] University of Delaware, Department of Physics and Astronomy, Bartol Research Institute, Newark, DE, USA

[91] University of Wisconsin-Madison, Department of Physics and WIPAC, Madison, WI, USA

——

[a] Louisiana State University, Baton Rouge, LA, USA

[b] also at University of Bucharest, Physics Department, Bucharest, Romania

[c] School of Physics and Astronomy, University of Leeds, Leeds, United Kingdom

[d] now at Agenzia Spaziale Italiana (ASI). Via del Politecnico 00133, Roma, Italy

[e] Fermi National Accelerator Laboratory, Fermilab, Batavia, IL, USA

[f] now at Graduate School of Science, Osaka Metropolitan University, Osaka, Japan

[g] now at ECAP, Erlangen, Germany

[h] Max-Planck-Institut für Radioastronomie, Bonn, Germany

[i] also at Kapteyn Institute, University of Groningen, Groningen, The Netherlands

[j] Colorado State University, Fort Collins, CO, USA

[k] Pennsylvania State University, University Park, PA, USA

Acknowledgments

PoS(ICRC2023)278